



In-situ

3D printing of diamond-coated carbon fiber reinforced polymer composites

Keywords: Carbon fiber, 3D printing, Diamond, Carbon fiber, Polymer matrix, Carbon fiber, Polymer matrix, Carbon fiber, Polymer matrix



Gemological Institute, China University of Geosciences, Wuhan 430074, PR China
 Hubei Gem and Jewelry Engineering Technology Research Center, Wuhan 430074, PR China
 School of Materials Science and Engineering, Huazhong University of Science and Technology, Wuhan 430074, PR China
 Mechanical Engineering, University of Birmingham, Birmingham B15 2TT, UK
 School of Electrical and Electronic Engineering, Huazhong University of Science and Technology, Wuhan 430074, PR China
 WMG, Materials Engineering Centre, University of Warwick, CV4 7AL Coventry, UK

ARTICLE INFO

Keywords:

Carbon fiber, 3D printing, Diamond, Carbon fiber, Polymer matrix, Carbon fiber, Polymer matrix, Carbon fiber, Polymer matrix

ABSTRACT

Carbon fiber reinforced polymer (CFRP) composites (3DG) were prepared by 3D printing of diamond-coated carbon fiber (DC-CF) and polymer matrix (PM) using selective laser melting (SLM). The DC-CF was prepared by chemical vapor deposition (CVD) of diamond on carbon fiber (CF). The 3DG composites were prepared by SLM of DC-CF and PM. The 3DG composites were characterized by scanning electron microscopy (SEM), energy-dispersive X-ray (EDS), X-ray diffraction (XRD), and mechanical testing. The results show that the 3DG composites have a high tensile strength of 478 MPa and a high modulus of 2.7 GPa. The 3DG composites also have a high thermal stability of 32.3 B and a high electrical insulation of 2–18 GHz. The 3DG composites are suitable for high-performance applications.

1. Introduction

Graphene (sp^2) is a two-dimensional carbon-based material with a hexagonal lattice structure. It has a high tensile strength of 2630 N m⁻¹ [1], a high modulus of 10⁵ N m⁻² V⁻¹ [2], and a high thermal conductivity of 5000 W m⁻¹ K⁻¹ [3]. Graphene is a promising material for high-performance applications. However, graphene is difficult to process and integrate into composites. Recently, diamond-coated carbon fiber (DC-CF) has been developed as a high-performance material. DC-CF has a high tensile strength of 99.7% [4] and a high modulus of 0.6 N m⁻² [4]. DC-CF is suitable for high-performance applications.

(2DG), 5, 6, 7, 8, 9, 10, 11, 12, 13, 14, 15, 16. B

*Corresponding author. E-mail address: gem@cgig.cug.edu.cn (G. Gem).

. T (, , fi
) , fl fi
(, ,) 3DG. B ,
3DG w
(, ,). H w
ffi
N
3DG w
fi 17,18
H , w
3DG w
19
S (SLM),
(AM) ,
(3D)
w , ffi
fl *in-situ* T ,
SLM T 20 ,
21 , N 22 . C w /
C w N
w
CVD w (< 0.001 . %) w
w , w
23 . W N
(> 0.1 . %) 17 , fi
24 . H w
SLM ffi
w
fl w w
(1000–1100). F ff
SLM 25 .
T , w fi
3DG/ (3DG/C)
SLM w CVD w
A w
SLM

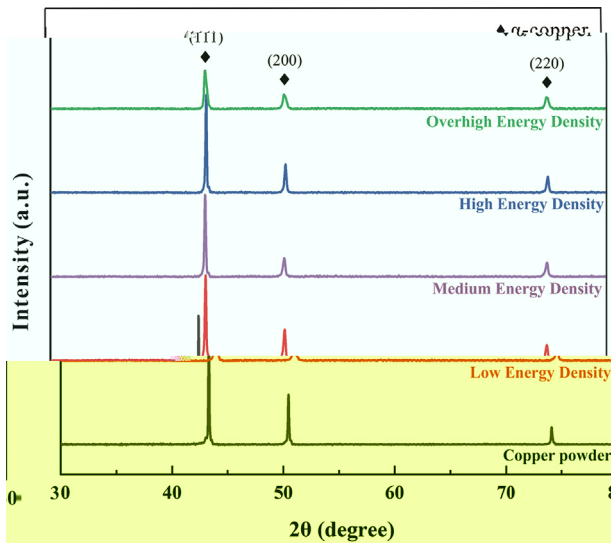


Fig. 3. RD patterns of copper powder at different energy densities. (a) Overhigh energy density, (b) High energy density, (c) Medium energy density, (d) Low energy density.

3.1.2. Formation of anisotropic microstructure under different volumetric energy density

The XRD patterns of the SLM copper powder at different energy densities are shown in Fig. 3. The peaks at $2\theta = 43.32^\circ$, 50.45° , and 73.52° correspond to the (111), (200), and (220) planes of copper powder, respectively (Fig. 3). The intensity of the (111) peak is significantly higher than that of the (200) and (220) peaks, indicating a strong texture along the (111) plane. The texture becomes more pronounced as the energy density increases from low to overhigh.

The microstructures of the SLM copper powder at different energy densities are shown in Fig. 4. The microstructures are characterized by the presence of un-melted powder, voids, inter-layer voids, gas holes, fish-scale like defects, pore chains, and irregular voids. The microstructures become more porous and irregular as the energy density increases from low to overhigh. The porosity of the SLM copper powder at different energy densities is summarized in Table 1.

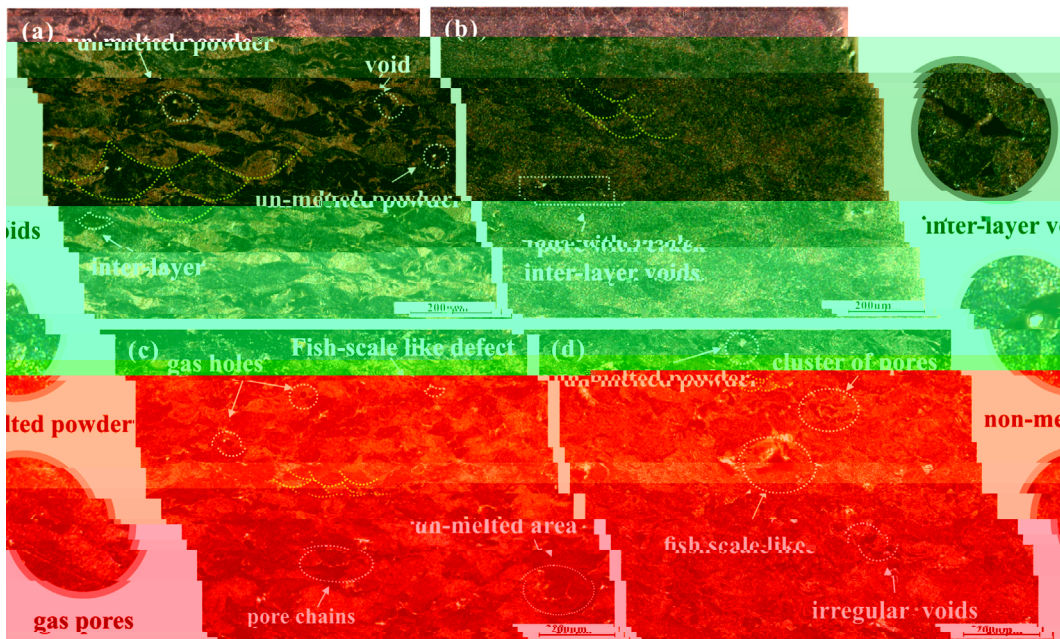


Fig. 4. Optical micrographs of the SLM copper powder at different energy densities: (a) 128 J/cm³, (b) 857 J/cm³, (c) 285 J/cm³, (d) 3000 J/cm³. (a) and (b) are at 200 μm scale, (c) and (d) are at 70 μm scale.

... ..

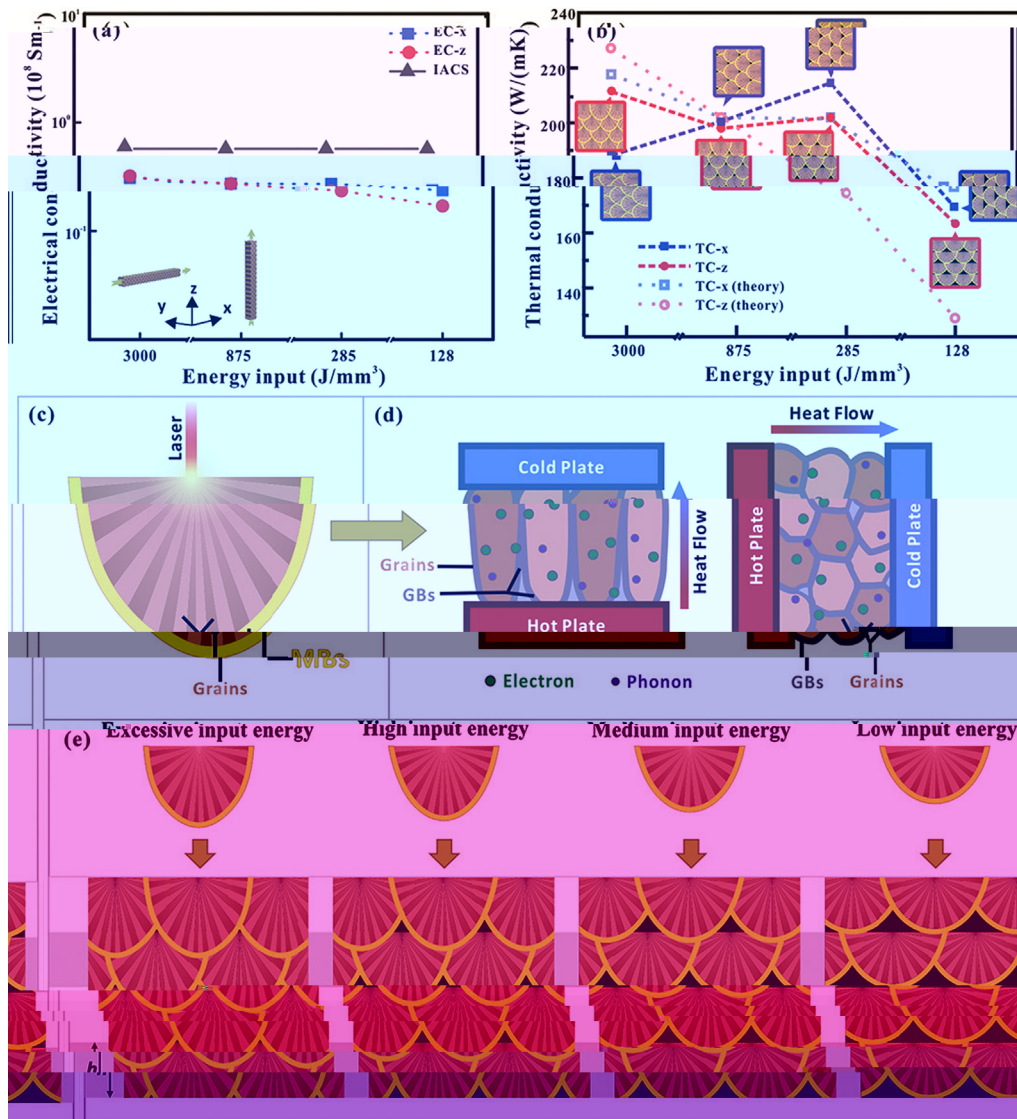


Fig. 7. (a) Electrical conductivity of EC-x, EC-z, and IACS. (b) Thermal conductivity of TC-x, TC-z, and their theoretical values. (c) Schematic of laser irradiation on a substrate. (d) Schematic of heat flow through grains and grain boundaries (GBs) between hot and cold plates. (e) Schematic showing the effect of excessive, high, medium, and low input energy on the microstructure.

in-situ CVD

39. A

33 V

(25 V)

39. U

40

23

41

CVD-

SEM, w

3DG/C

450 μm (Fig. 8a). A

(Fig. 8b),

EDS

(Fig. 8c-d), w

(Fig. 8e-g). T

3DG/C

(Fig. 8h).

3DG/C

(~1590 °C⁻¹) w

2D- (2699 °C⁻¹)

G- (~1590 °C⁻¹) w

42 (Fig. 8). S

D- (~1350 °C⁻¹) fl

43, D G (I_D/I_G) w

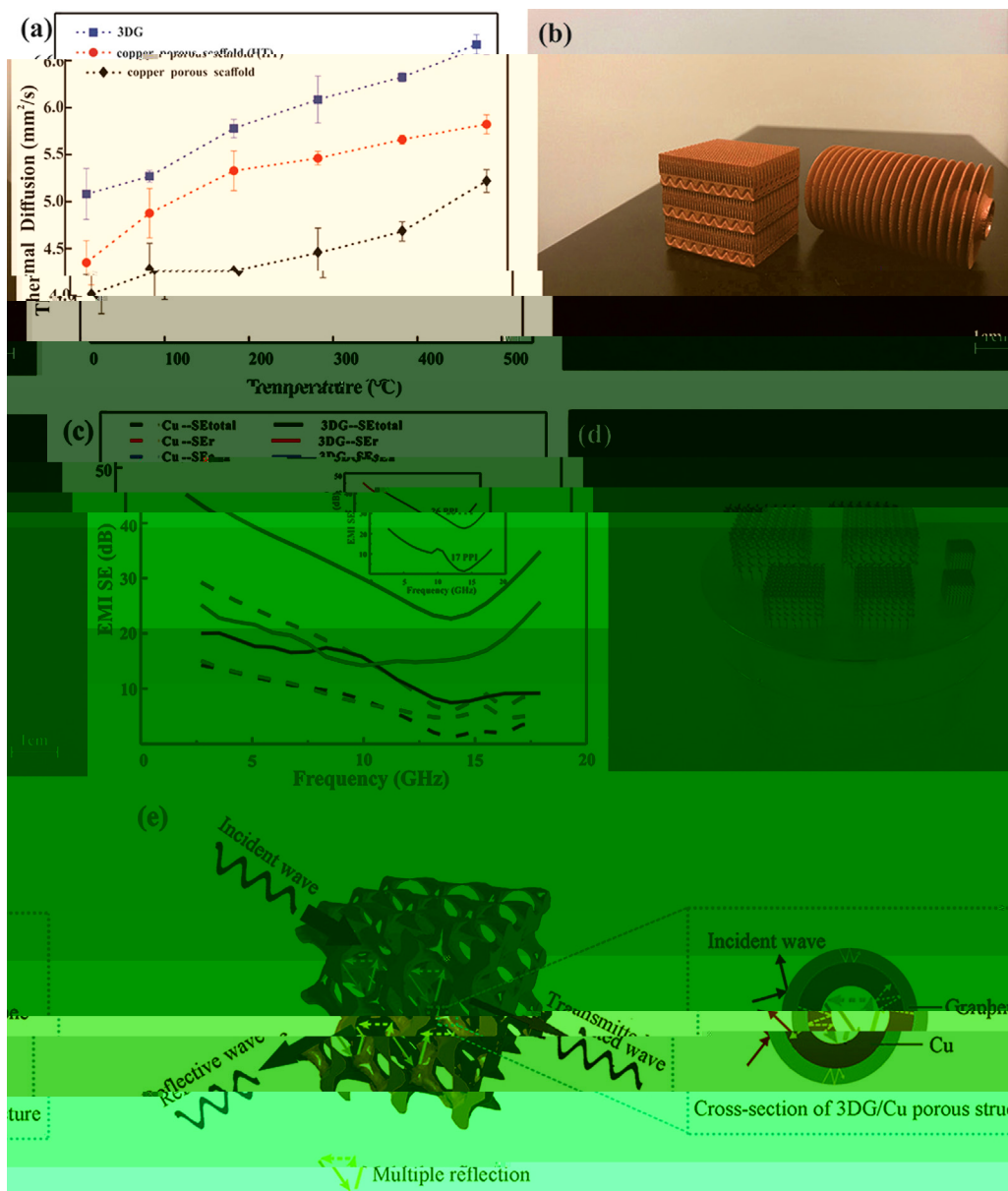


Fig. 9. (a) Thermal Diffusion (mm²/s) vs Temperature (°C) for 3DG (□), copper porous scaffold (●), and copper porous scaffold (◆). (b) 3D models of 3DG and copper porous scaffold. (c) EMI SE (dB) vs Frequency (GHz) for Cu-SEtotal (—), Cu-SEr (---), Cu-SEloss (· · ·), 3DG-SEtotal (—), 3DG-SEr (---), and 3DG-SEloss (· · ·). (d) Schematic of 3DG/Cu porous structure. (e) Multiple reflection diagram showing incident, reflective, and transmitted waves.

Table 1

Coating materials	Substrate	Method	Maximum shielding efficiency (dB)	Improvement of thermal property (%)	Ref
G	G	I	37	—	50
G	PS	H	29.3	—	56
G	PMMA	S	19	—	57
C /G	A	S	—	8.5	58
G	N	F	—	554	59
G	C-N	E	20	—	60
G	C	P	—	2.4	61
G	C	F	47	6.3	62
G	C	CVD + SLM	47.8	27	T

Note: (□) -PPMA, (●) -PS.

HT
in-situ w (F. 9a). S
 3DG/C ff
 HT
 1-2
 W
 SLM
 fl w (w fl) 500 μm
 (F. 9b),
 G
 (T. 1). I
 O
 N
 T
 EMI, EMI SE, w 3DG/C ff
 (EM) w
 2-18 GHz (F. 9c),
 W *in-situ* w
 ff SE 15.9 32.3 B, w
 47.8 B (88.2%),
 20 B. T
 3DG/C fi w
 J K 44 EMI
 w T EMI SE
 133% w
 (,) 20 110 PPI ().
 R K 45 w EMI
 W
 17 26 PPI (F. 9c insert) 105%
 EMI SE. I w EMI
 ff w SLM. T
 3DG/C 26 PPI EMI SE
 32.3 B, 99.9% EMI w T
 60
 (30 ff) 46 T EMI
 3DG/C w
 T 1. I EMI SE
 3DG/C w
 3D
 T EMI fl (SE_r),
 (SE_a) fl (EM) w 47,
 w
 48 R 49 w
 w, w
 T w EM w
 fi
 50 R EMI
 T
 w w w
 w fi C 51 F
 w
 52 S O₂ 53 W
 3DG/C ff w

SE_r, SE_a, w F. 9e. W w
 w 3DG/C ff
 w w fl w ff S
 3DG/C
 fi
 w w T
 EM w fi w w
 w EM w
 SE_r, O
 w ff, w w fi EM
 w ff EM
 T
 ff w
 w J 54 I w
 fi w
 fl ff M
 w
 w fl
 EM w
 EM w T w
 w 44 T
 w 3D EM w w
 I CVD
 R S 3.3
 55 I
 EM w w w
 O w
 3DG/C
 fi w fi
 T
 w ff

4. Conclusions

A 3DG/C ff w w
in-situ CVD
 T w
 ff W
 3DG/C
 EMI SE
 15.9 () 32.3 B,
 47.8 B (88.2%), w 26.8%
 ff T 3DG/C
 ff fl fi
 T EMI
 3DG/C ff
 EMI

Credit authorship contribution statement

Kaka Cheng: C, M, F, W
 Wei Xiong: V, I, W
 Yan Li: W &, F
 Liang Hao: F, Chunze Yan: R, F
 Zhaoqing Li: V, Zhufeng Liu: F
 Yushen Wang: I, S, Khamis Essa: W &, Li Lee: D, Xin Gong: S
 Ton Peijs: W &, S

Declaration of Competing Interest

The authors declare that they have no competing interests.

Acknowledgement

The authors thank the National Natural Science Foundation of China (No. 51671091, No. 51902295, No. 51675496). T. F. and R. F. thank the University of Umeå (Sweden) (No. CUG170677). H. P. and N. S. thank the National Natural Science Foundation of China (No. 2019 CFB264).

Appendix A. Supplementary data

Supplementary data associated with this article can be found in the online version at <https://doi.org/10.1016/j.cmi.2020.105904>.

References

- Berg, N., N. M., K. M., S. G., P. M., S. 2018;91:24–69.
- B. AA, G. S, B. W, C. L, T. W. D, M. F, S. 2008;8(3):902–7.
- L. H, C. M, P. W, H. P, O. S, G. 2016;8(36):24112–22.
- K. M, K. J, J. B, C. K, J. H, A. J. H. G. ACS N 2017;11(8):7950–7.
- P. C, M. H, M. T, M. L, D. P. A. C. B 2020;262:118266–76.
- L. J, W. C, L. J, S. H, W. G, L. F, C. G. 2017;101:50–8.
- H. Q, L. S. W, C. L. H, J. S. H, H. Q. S. 2018;6(42):21216–24.
- D. T. M, S. P, D. P, K. J, K. W, M. A. T. 3D 2017;1(4):467–70.
- Q. L, L. L. T. RSC A 2014;4(72):38273–80.
- D. H, L. S. P, N. W, J. G. 3D M S₂ 2016;90:424–32.
- L. L, W. S, C. Q, H. M, K. H. L, D. W, S. 3D w. EM 2018. // /10.1002/ 201803938.
- L. J, P. C, R. G, N. D, G. ACS N 2013;7(7):6001–6.
- J. S. H, A. W, S. G, A. L. W. A. W. C. I. E 2017;56:15520–38.
- I. T, S. W, K. K, M. T, T. T, K. T. PCCP 2018;20(9):6024–33.
- S. K, D. N, M. C, V. N, E. J. T. J. E. S 2002;149(8):370–7.
- C. H, S. M, S. W. H, L. G, H. Q. P. 3D w. S 2011;7(22):3163–8.
- K. H, G. M, J. I, H. J, W. C, C. M. U. M 2019;1(4):1077–87.
- S. Q, F. L, W, L. H, L. C. A. M 2017;29(31):1701583–90.
- G. C, L. T, H. D, W. T. ACS N 2019. // /10.1021/ 9 08191.
- C. C, H. B, N. J, C. S, L. F. 3D T 6A 4V. M. D 2019;175:107824–33.
- S. J, B. J. D. T. ff. NB. 316L. SLM. S. C. T. 2016;307:407–17.
- R. DC, HB, L. J, L. S. J, J. W, R. M. T. N. M. S. E. A. S. 2020;771:138586–95.
- L. C, W. A, J. K. S, N. J, D. L. S. 2009;324(5932):1312–4.
- C. P, R. W. C, G. L. B, L. P. S. E, C. H. M. T. w. w. N. M. 2011;10:424–8.
- J. S. D, D. S, G. L, K. J. P, H. J. V, V. K. I. J. M. P. T. 2019;270:47–58.
- W. H, L. L, T. D, C. Q, F. Eff. 2019;170:107697–708.
- G. D. D, M. W, W. K, P. w. R. L. I. M. R. 2013;57(3):133–64.
- L. E, T. S, C. L, F. A. Eff. 316L. (SLM) 2017;249:255–63.
- S. W, L. J, W. P, C. T 6A 4V. A. P. A. M. S. P. 2018;124:685–98.
- L. M. S, D. W, S. C. I. AS 316L. w. M. D. 2015;87:797–806.
- L. CLA, M. S, T. w. M, A. w. RC, W. P. J, L. P. D. T. ff. w. A. M. 2019;166:294–305.
- T. K, T. W. Q, T. J, D. M, M. D, R. α/β. T 6A–4V. S. R. 2016;6:26039–48.
- K. H, T. P, L. N. H, T. S. B, C. K. G. T 6A–4V. V. P. P. 2016;11(3):183–91.
- R. H. K, K. N. V, G. H, S. T. L, S. B. E. M. 6 4. J. M. E. P. 2013;22(12):3872–83.
- T. K, T. J, V. G, P. Q. G. A. T 6A–4V. J. A. C. 2015;646:303–9.
- R. DA, M. L. E, M. H. N. A. M. 2011;59(10):4088–99.
- W. H. Eff. C–2.4N–0.7S. J. A. C. 2018;743:258–61.
- K. S. W. S. E. 2003;23:309–48.
- L. G, G. J. ff. R. G. N. P. E. C (111). N. L. 2010;10(9):3512–6.
- L. S, C. W. W, C. L. R. ff. R. S. E. w. N. C. 2009;9(12):4268–72.
- W. C, W. H, S. Q. L. A. C. 2020;161:479–85.
- F. AC, M. J. C, V. C. C. L. M. M. F. R. P. R. L. 2006;97(18):187401–4.
- S. G, J. S. H, F. P. C, H. H. Q. F. M. L. 2017;200:97–100.
- J. K, H. J, C. J, D. F. C–N. w. CNT. A. S. S. 2014;311:351–6.
- R. K, M. DP, A. C, M. S, S. K. E. EMI. P. A. 2018;12:475–84.
- S. B, L. W, W. C. (EMI). ACS. A. M. I. 2016;8(12):8050–7.
- L. N, H. D. F, H. L. G. 964.535.80S, JC, 31.4(341

M 2019;34(5):489–98.

53 W B, C M, L M. R [https://doi.org/10.1016/j.compositesa.2014.06.011](#). *Composites Part A* 2014;26:3484–9.

54 C H, W S, J J, C J, S J. *Composites Part A* 2019;121:139–48.

55 W L, J Q, T ff MWCNT *Composites Part A* 2015;26(3):1895–9.

56 D P, GR, H P, Q F, M B, ML. *Composites Part A* 2012;22:1877–4.

57 HB, Q, WG, H, T *Composites Part A* 2011;3:918–24.

58 S A, U N, T V. T *Composites Part A* 2016. [https://doi.org/10.1051/compta/2016021](#).

59 P MT, J H, R ff RS, S L. T *Composites Part A* 2012;12:2959–64.

60 J K, H, H, D P, C-N *Composites Part A* 2017;122:244–7.

61 R H, L S, B S, K TW, L DS, L HJ, T *Composites Part A* 2015. [https://doi.org/10.1038/ncomms12710](#).

62 T, F SG, L G, Q, L G, R KP, S *Composites Part A* 2020. [https://doi.org/10.1016/j.compositesa.2019.105670](#).

63 R DA, M LE, M E, H DH, M JL, M BI, N *Composites Part A* 2011;59(10):4088–99.

64 E SF, L KG, S VK, M IC. T *Composites Part A* 1973;1(1):10–38.